Weather and Climate Extremes 40 (2023) 100559

Contents lists available at ScienceDirect

Weather and Climate Extremes

journal homepage: www.elsevier.com/locate/wace

Global cropland exposure to extreme compound drought heatwave events under future climate change

Anqian Wang [a], Hui Tao [b,*], Gang Ding [c], Baolei Zhang [a], Jinlong Huang [d], Quanyuan Wu [a]

[a] College of Geography and Environment, Shandong Normal University, Jinan, 250358, China
[b] State Key Laboratory of Desert and Oasis Ecology, Xinjiang Institute of Ecology and Geography, Chinese Academy of Sciences, Urumqi, 830011, China
[c] Risk Monitoring and Comprehensive Disaster Reduction Division, Department of Emergency Management of Xinjiang Uygur Autonomous Region, Urumqi, 830011, China
[d] Collaborative Innovation Center on Forecast and Evaluation of Meteorological Disasters/Institute for Disaster Risk Management/School of Geographical Science, Nanjing University of Information Science and Technology, Nanjing, 210044, China

ARTICLE INFO

Keywords:
Compound drought heatwave events
Cropland exposure
CMIP6
Global and continent

ABSTRACT

The risk of compound drought heatwave events (CDHEs) and their persistence has intensified in recent decades and is expected to increase faster in the future. Projecting future changes in the CDHEs and the area of the cropland exposed to CDHEs under different scenarios is critical for climate adaptation and sustainable development. In this study, we analyze cropland exposure to extreme CDHEs at the global and continental scales under different Shared Socioeconomic Pathways (SSPs) scenarios for the mid-term (2041–2060) and long-term (2081–2100) of the 21st century by using 14 CMIP6 GCMs and LUH2 land-use data. We find that the extreme CDHEs with high frequency are mainly located in tropical areas. The frequency of extreme CDHEs in the future will be much higher than that of the baseline period (1995–2014), and the increased frequency will be more obvious with the emissions increase. Overall, the global total cropland exposure in warm season during the 1995–2014 period will be 148.05 $\times$ 10^3 km^2 $month^{-1}$. Exposure in the mid-term and long-term will be 868.68–1801.25 and 1058.58–3887.54 $\times$ 10^3 km^2 $month^{-1}$ under the different SSP scenarios. The climate effect will be the dominant driving factor for the increase in cropland exposure. Cropland exposure to extreme CDHEs will increase on all continents, especially in Asia and Africa. Our findings provide scientific evidence of the benefit of limiting low-emission scenarios which will effectively reduce cropland exposure to CDHEs under future climate change.

1. Introduction

Climate change is one of the most serious threats to human society in the 21st century and may generate more extreme weather events and show an increasing trend at regional and global scales under anthropogenic climate change (AghaKouchak et al., 2014; Leonard et al., 2014; Zscheischler et al., 2020; IPCC, 2021). Extreme weather and climate events are often triggered by complex atmospheric physical processes and can cause disasters that contribute to severe socioeconomic risk (Zscheischler et al., 2020). These impacts may not be uniquely determined by a single extreme but may be related to compound extreme weather and climate events that have high impacts, an idea first introduced by the special report on managing the risks of extreme events and disasters to advance climate change adaptation (SREX), which released by the Intergovernmental Panel on Climate Change (IPCC) (AghaKouchak et al., 2014; Leonard et al., 2014; Zscheischler et al., 2020). Compound extreme weather and climate events can be defined as the combination of two or more extreme events that occur concurrently or sequentially (AghaKouchak et al., 2014; Leonard et al., 2014; Zscheischler et al., 2020; Zhang et al., 2021a). Compared with individual extreme events, compound extreme events often have substantially amplified harmful impacts, leading to much more severe ecological and socioeconomic damage (Hao et al., 2020; Weber et al., 2020; He et al., 2022b; Zhang et al., 2022a).

Among the multiple compound weather and climate events, compound drought heatwave events (CDHEs) are one of the most typical compound extreme events that have attracted increasing attention (Mazdiyasni and AghaKouchak, 2015, 2020; Feng et al., 2019; Alizadeh

* Corresponding author.
E-mail address: taohui@ms.xjb.ac.cn (H. Tao).

https://doi.org/10.1016/j.wace.2023.100559
Received 7 June 2022; Received in revised form 16 December 2022; Accepted 25 March 2023
Available online 27 March 2023

et al., 2020; Mukherjee et al., 2020; Liu et al., 2021; Tang et al., 2022; Wu and Jiang, 2022; He et al., 2022a, 2022b; Li et al., 2022; Libonati et al., 2022). Drought and heatwave are two kinds of disasters with a high frequency and wide range in the world and are also the most obviously affected by climate change. The relationship between the temperature and the precipitation is negative, influenced by the land-atmospheric feedback (Zscheischler and Seneviratne, 2017). The occurrence of a heatwave would inhibit the precipitation generation, increase the sensible heat flux, which could further lead to the surface temperature increase, accelerate the soil moisture evaporation, and finally aggravate drought severity (Seneviratne et al., 2010; Miralles et al., 2019).

Previous studies have shown more frequent CDHEs in recent decades globally (Alizadeh et al., 2020; Liu et al., 2021). In the USA, compound drought heatwave events increased with a statistically significant shift in their distribution during 1960–2010 (Mazdiyasni and AghaKouchak, 2015). A similar phenomenon is found in China, where the events have become more frequent and widespread, especially since the late 1990s (Yu and Zhai, 2020a), with a large population exposed to CDHEs (Liu et al., 2021; Zhang et al., 2021b). Due to the combined effects of long-term trends of global warming and multi-time scale variability, CDHEs will increase under the influence of climate change and will be projected to further increase in the future (Hao et al., 2018; Liu et al., 2021). According to Liu et al. (2021), population exposure to severe CDHEs under 2.0 °C and 3.0 °C global warming relative to the preindustrial level will increase by 108 and 266 million, respectively, compared with the 1.5 °C global warming.

The harmful impact is not only on population, but also on crop growth, produce serious economic losses, and has a serious impact on food security (Zscheischler et al., 2018; Feng et al., 2021; He et al., 2022a). Agricultural production is mainly determined by meteorological factors such as temperature and precipitation, and climate variation explains a third of global crop yield variability (Ray et al., 2015). Drought and heatwave are among the most detrimental climate extreme with a variety of direct, indirect, immediate, and delayed impacts (Mazdiyasni and AghaKouchak, 2015). The drought and extreme heat significantly reduced national cereal production by 9–10% (Lesk et al., 2016; Alizadeh et al., 2020). Drought mainly reduce the yield by slowing down photosynthesis and shortening the growth season (Lesk and Anderson, 2021), while the heatwave can not only directly affect the crop growth by reducing pollen viability and damaging tissues, but also indirectly reduce the yield by decreasing soil moisture and causing drought through evapotranspiration (Siebert et al., 2017; Lesk and Anderson, 2021). The impact of CDHEs on cropland at the global and continental scales has not been discussed carefully, though this information is critical to preparing for and mitigating their negative effects on agricultural production, which are closely related to human well-being and social stability (Hu et al., 2020; Potapov et al., 2022).

Traditionally, drought events are described by monthly drought indices (i.e., the standardized precipitation evapotranspiration index (SPEI) and standardized precipitation index (SPI) (McKee et al., 1993; Vicente-Serrano et al., 2010), while heatwaves (or hot extreme events) are often defined by using the absolute or relative threshold temperature on daily scales as a period of consecutive extremely hot days (Wang et al., 2020; Zhang et al., 2021b; Luo et al., 2022). Therefore, how to combine the two kinds of disasters with different time scales is the primary problem in exploring CDHEs (Mukherjee et al., 2020; Yu and Zhai, 2020a; Zhang et al., 2021b). With the development of research, scholars have attempted to directly describe the CDHE by using one index, such as the standardized dry and hot index (SDHI) (Hao et al., 2018; Wu et al., 2020; Liu et al., 2021; Tang et al., 2022), standardized compound event indicator (SCEI) (Hao et al., 2019), and compound drought-hot extreme index (CDHI) (Hao et al., 2020).

In the present paper, we present the CDHEs by using the SDHI and project cropland exposure in the global and continental scales under the mid-term and long-term period of the 21st century, based on 14 GCMs outputs and cropland area projection. The main target of this paper is to improve our understanding in the projection of CDHEs and the impacts of climate drives to the CDHEs under various future scenarios, which will provide support about the risk assessment, adaptation, and mitigation strategies under climate change. The rest of this paper is organized as follows: Section 2 describes the datasets and methods used in this study. The results are presented in Section 3. In Section 4, we present some discussions and conclusions.

2. Data and methods

2.1. Data

2.1.1. Climate data

Global monthly temperature and precipitation data are extracted from the Climatic Research Unit (CRU) datasets with a spatial resolution of 0.5° × 0.5° for the period 1961–2014, which were generated based on data from more than 4000 meteorological stations around the world (Harris et al., 2020; Wang et al., 2020; Liu et al., 2021).

The monthly air temperature and precipitation outputs during 1961–2100 of 14 global climate models (GCMs) are from the Coupled Model Intercomparison Project Phase 6 (CMIP6) (Table 1). The GCM temperature and precipitation are divided into two periods: before 2014 (including 2014) is the historical period, and after 2014 is the projection period. The historical scenario used in this study has all-forcing simulations, which are forced by both anthropogenic and natural forcing (Zhang et al., 2022b). Four scenarios including SSP1-2.6, SSP2-4.5, SSP3-7.0, and SSP5-8.5, are used in this research, belonging to Tier-1 experiments. Tier-1 experiments are the core experiments, designed to provide a full range of forcing targets (Eyring et al., 2016; Gidden et al., 2019; Hofer et al., 2020; Liu et al., 2021; Ma and Yuan, 2021; Ullah et al., 2022).

The period 1995–2014 is considered the baseline period in the 6th Assessment Report (AR6) of the IPCC, and the 21st century has been divided into three periods, i.e., the near-term (2021–2040), the mid-term (2041–2060) and long-term (2081–2100) (IPCC, 2021).

Temperature and precipitation data of GCMs have been bias-corrected based on the CRU data by using the equidistant cumulative distribution function (EDCDF) method and downscaled to 0.5° × 0.5° by using the spatial disaggregation (SD) method (Li et al., 2010). Comparing the CRU and GCM, we find that the precipitation of GCMs is overestimated in most regions of the world, while it is slightly underestimated in South America. In terms of temperature, GCMs slightly underestimate in many parts of the world. After bias correction, the precipitation and temperature of the GCMs become close to the observed values (Figs. S1–S3).

2.1.2. Land-use data

The Land Use Harmonization Version 2 (LUH2) dataset is used to

Table 1
Description of the global climate models.

Climate Model	Institute ID	Country	Resolution (grid points)
BCC-CSM2-MR	BCC	China	160 × 320
CAMS-CSM1-0	CAMS	China	160 × 320
CESM2	NCAR	USA	192 × 288
CESM2-WACCM	NCAR	USA	192 × 288
CNRM-CM6-1	CNRM-CERFACS	France	128 × 256
CNRM-ESM2-1	CNRM-CERFACS	France	128 × 256
CanESM5	CCCma	Canada	64 × 128
FGOALS-g3	CAS	China	80 × 180
GFDL-ESM4	NOAA-GFDL	USA	180 × 288
IPSL-CM6A-LR	IPSL	France	143 × 144
MIROC-ES2L	MIROC	Japan	64 × 128
MIROC6	MIROC	Japan	128 × 256
MRI-ESM2-0	MRI	Japan	160 × 320
UKESM1-0-LL	MOHC	UK	144 × 192

represent historical and future land-use activities in the world during 850–2100 (Chen et al., 2020b; Hurtt et al., 2020; Ma et al., 2020; García-Peña et al., 2021; Song et al., 2021). It is a new historical and projected future land-use forcing dataset for CMIP6 (Eyring et al., 2016). LUH2 was developed based on the Historical Database of the Global Environment (HYDE) and multiple future scenarios following the Shared Socioeconomic Pathways (SSPs) (Chen et al., 2020b; García-Peña et al., 2021). It provides global gridded fractional land-use patterns, underlying land-use transitions, key agricultural management information, and resulting secondary land data from 850 to 2100 with spatial resolution of 0.25° × 0.25° and temporal resolution of 1 year (Hurtt et al., 2020). In addition, LUH2 classifies the land into 5 land-use types (cropland, pasture, primary, secondary and urban) and 12 sub-types. The sum of C3 annual cropland, C3 perennial cropland, C4 annual cropland, C4 perennial cropland, and C3 nitrogen-fixing cropland is used to denote cropland.

2.2. Methods

2.2.1. Defining the compound drought heatwave event

The SDHI is relatively simple and effective in describing the CDHEs, and has been widely used in many regions of the world (Hao et al., 2018; Wu et al., 2020; Liu et al., 2021; Tang et al., 2022). The original version of the SDHI used the ratio of the marginal probability or percentile of precipitation and temperature to evaluate the relative status of dry and hot conditions. However, the drought condition is also influenced by the temperature and evapotranspiration, and thus it is insufficient to describe the drought trends under the warming climate by using only precipitation (Vicente-Serrano et al., 2010; Zhou et al., 2020). Therefore, in this study, the difference between precipitation and potential evapotranspiration (PET) is used to present drought conditions, a concept similar to the SPEI (Vicente-Serrano et al., 2010). The PET is calculated based on the Thornthwaite method (Thornthwaite, 1948).

Thus, to incorporate the comparative status of both moisture and heat conditions, we define a matrix as follows:

$$X = \frac{G_1(P - PET)}{G_2(T)} \tag{1}$$

where functions $G_1(P - PET)$ and $G_2(T)$ are the percentile distribution functions of precipitation minus potential evapotranspiration and temperature, respectively.

We termed the index as SDHI, in which a marginal cumulative distribution F was first fitted, and then the standardization was performed based on the standard normal distribution ϕ. The smaller the SDHI value, the more severe the CDHEs. The intensity of CDHEs can be further categorized by using different SDHI thresholds. If the SDHI is lower than −0.5, CDHEs can be considered, and −0.8, −1.3, −1.6, and −2.0 are the thresholds of moderate, severe, extreme, and exceptional CDHEs, respectively (Hao et al., 2018; Liu et al., 2021).

$$SDHI = \phi^{-1}[F(X)] \tag{2}$$

Marginal distribution functions (i.e., F) are used as an empirical method based on the Gringorten plotting position formula (Gringorten, 1963) to compute the following:

$$F = \frac{(i - 0.44)}{(n + 0.12)} \tag{3}$$

where i is the rank and n is the length of observations.

We focus on the CDHEs in the warm season, which is defined as the hottest three months in each grid (Zscheischler and Seneviratne, 2017). To avoid CDHEs appearing in high-mountain and polar regions, we consider that a monthly temperature above 20 °C is the basic condition for CDHEs.

2.2.2. Thornthwaite method

The Thornthwaite method is widely used and the simplest approach to calculate the PET, which correlates the mean monthly temperature with PET as determined by the water balance with the supply of surface water (Thornthwaite, 1948).

The implementation of Thornthwaite's original approach is slightly modified (Willmott et al., 1985), where Thornthwaite's parameterization is used for a limited range of temperature values,

$$PET = \begin{cases} 0 & T < 0^\circ C \\ 16\left(\frac{10T}{I}\right)^a & 0C \le T < 26.5^\circ C \\ -415.85 + 32.24T - 0.43T^2 & \ge 26.5^\circ C \end{cases} \tag{4}$$

where I is the heat index, and a is the parameterization determined by a third-order polynomial.

$$I = \sum_{i=1}^{12} \left(\frac{T}{5}\right)^{1.514} \tag{5}$$

$$a = 6.57 \times 10^{-7} I^3 - 7.71 \times 10^{-5} I^2 + 1.7921 \times 10^{-2} I + 0.49239 \tag{6}$$

Finally, to account for variable day and month lengths, the PET is adjusted:

$$PET = PET\left(\frac{\theta}{30}\right)\left(\frac{h}{12}\right) \tag{7}$$

where θ is the length of the month (in days), and h is taken as the duration of daylight (in hours) on the 15th day of the month. The latter correction ensures that the Thornthwaite parameterization for PET is related to the latitude of the site considered, next to the monthly means of daily averaged temperature.

2.2.3. Relative importance of climate and land-use changes on exposure

The cropland exposure is calculated by multiplying the cropland area by the number of CDHEs at each grid point. As the CDHE is the monthly scale in this research, the unit of cropland exposure is $km^2 \cdot month^{-1}$ (Jones et al., 2015). For each GCM projection, the 20-year (length of baseline period, mid-term, and long-term) mean exposure is computed under different SSP scenarios. Finally, we aggregate grid exposure to global and continental scales.

The exposure change can be divided into three factors, namely, climatic effect, cropland effect, and interaction effect (Smirnov et al., 2016; Liu et al., 2017; Chen et al., 2018, 2020a; Jones et al., 2018; Weber et al., 2020; Zhang et al., 2021b; Das et al., 2022; Wang et al., 2022). To isolate the impact of cropland and climate change on cropland exposure, we have designed two additional experiments by holding the climate or cropland constant. The influence of climate on exposure is determined by allowing climate to change according to the model projection but leaving cropland at the baseline period level. The cropland effect is determined by allowing cropland to change but leaving the climate at the baseline period level. The difference between total exposure and the summation of climate and cropland effects is considered the interaction effect, which represents the simultaneous changes in climate and cropland (Smirnov et al., 2016). Therefore, the relative contributions of climate and cropland changes to the exposure can be obtained by dividing projected changes in exposure by the total exposure changes.

3. Results

3.1. Frequency of extreme CDHEs at the continental scale

Although the GCMs data used in this study are downscaled and bias-corrected, we compared the spatial distribution of the frequency of extreme CDHEs calculated by CRU (Fig. 1a), GCMs after bias correction

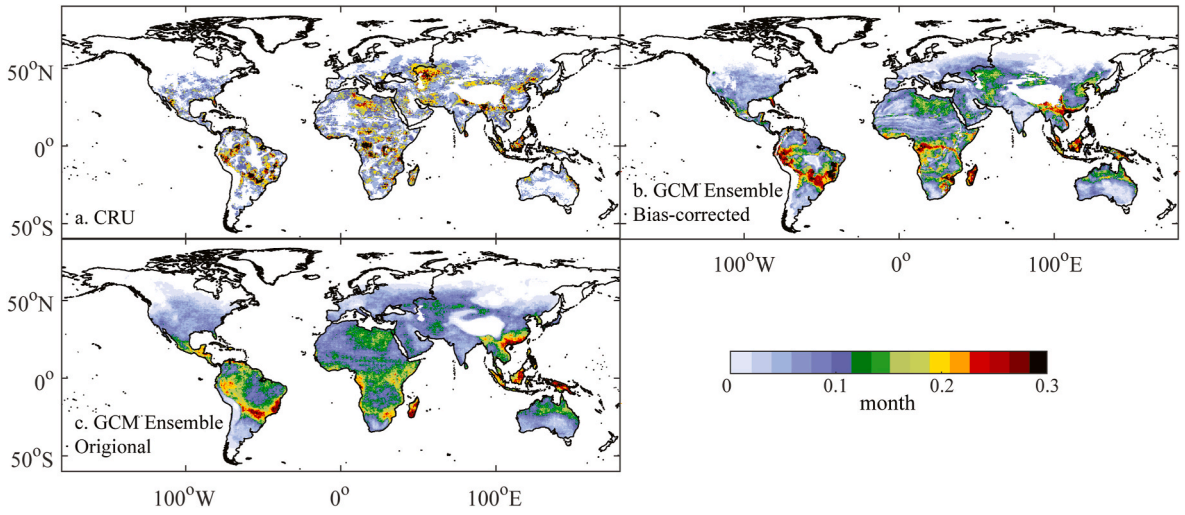

Fig. 1. Global spatial distribution of the frequency of extreme CDHEs during the baseline period by using the CRU data (a), the ensemble mean of 14 GCMs that have been bias-corrected (b), and original GCMs (c).

(Fig. 1b), and original GCMs data (Fig. 1c) in the baseline period to further assess the simulation ability of the GCMs.

The results show that there is no distribution of extreme CDHEs in high-altitude areas such as North America, northern Eurasia, and the Qinghai-Tibet Plateau. However, northern Africa, Southern China, and tropical areas are generally prone to extreme heat and drought events. The spatial correlation coefficient between the spatial distribution of extreme CDHEs of CRU and original GCMs data is 0.56 ($p < 0.05$), and the spatial correlation coefficient between CRU and GCMs after bias correction is 0.73 ($p < 0.05$), indicating that the original GCM has a certain ability to simulate extreme CDHEs, and the simulation ability of the GCMs is further improved after bias correction.

In this research, the frequency of extreme CDHEs in the grid on the continent scale was averaged over time and is presented in Fig. 2. In the baseline period, there were no extreme CDHEs in high-latitude and high-altitude areas, among which the proportions of North America, Asia, and Europe were 71.1%, 47.1%, and 50.0%, respectively (Fig. 1b). This result was mainly caused by the large areas on the three continents where temperatures are lower than 20 °C, which does not meet the prerequisites for CDHEs. Among the six continents, the average frequency of CDHEs is lowest in North America in the baseline period, followed by Europe and Asia. The largest frequency of extreme CDHEs appeared in Africa, followed by Oceania and South America.

In the middle of the 21st century, the temperature elevation in all continents further increased the frequency of drought and heatwave events, leading to more CDHEs. Moreover, the maximum frequency of extreme CDHEs in all continents will be much higher than that in the baseline period. The extreme CDHEs will increase with the increase in emission scenarios.

The frequency of extreme CDHEs in the long-term will be higher than that of corresponding scenarios in the mid-term. In the long-term, the frequency of extreme CDHEs on all continents under the SSP1-2.6 scenario will be basically the same as that in the mid-term, while the frequency of extreme CDHEs in other scenarios increase obviously. Among the 6 continents, the frequency in Africa and South America will be much higher than that in other continents, and North America will be the lowest (Fig. 1).

The spatial distribution of extreme CDHE frequency in the mid-term and long-term will be similar to the baseline period (Fig. S4). The proportion of continents without extreme CDHEs declines dramatically. In

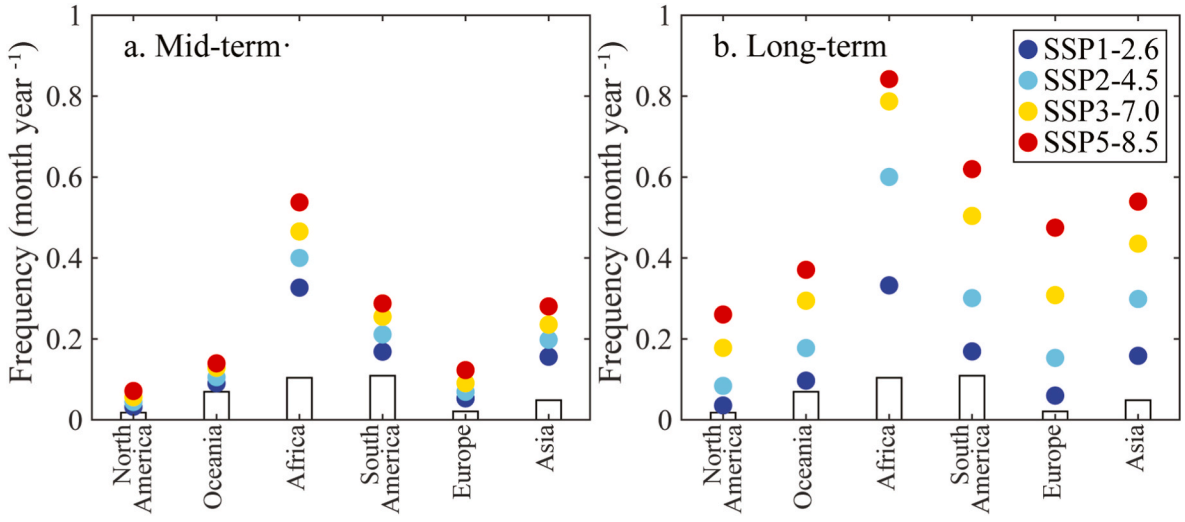

Fig. 2. The average frequency of extreme CDHEs to each continent in the baseline period and mid-term (a) and long-term (b) of the 21st century under different SSPs. The color means different SSPs, the white bar represents the baseline period. (For interpretation of the references to color in this figure legend, the reader is referred to the Web version of this article.)

the Middle East, North Africa, Central Africa, and some areas of northern South America, the warm seasons will all have extreme CDHEs. Moreover, extreme CDHEs will occur in northern North America and western Siberia, which have no extreme CDHES in the baseline period, especially under the SSP5-8.5.

3.2. Global cropland exposure in the baseline period

The spatial pattern of global cropland exposure to extreme CDHEs in the warm season, based on the multi-ensemble mean of GCMs during the baseline period (1995–2014) is shown in Fig. 3. Overall, the global total warm season cropland exposure during the 1995–2014 period was 148.05 $\times$ 10^3 km^2 $month^{-1}$, only accounting for 0.86% of the total cropland. Regions with high exposure are mainly distributed over East Asia (e.g., North China), Southeast Asia (e.g., Indonesia and Malaysia), and southern Brazil. These regions also have more cropland (Fig. 3b) and more months in the warm season (Fig. 1b). However, in regions with large croplands, such as Central Europe, western North America, and South Asia (Fig. 3b), cropland exposure to extreme CDHEs was low due to the lower frequency of extreme CDHEs. Exposure was also high near tropical areas in Africa due to the frequency of CDHEs and the cropland distribution. Cropland exposure to CDHEs is highest in Asia (67.27 $\times$ 10^3 km^2 $month^{-1}$), followed by Africa (31.17 $\times$ 10^3 km^2 $month^{-1}$) and South America (24.67 $\times$ 10^3 km^2 $month^{-1}$), and lowest in Oceania (1.87 $\times$ 10^3 km^2 $month^{-1}$). Cropland exposure in Europe and North America was 8.00 and 15.0 $\times$ 10^3 km^2 $month^{-1}$, respectively.

3.3. Spatial distribution of cropland exposure to CDHEs in the middle and long term

Considering that the CDHEs are becoming more severe in those regions that are already experiencing water shortages, we need to better assess the socioeconomic risks to support climate change mitigation under different scenarios.

The extreme CDHE cropland exposure will be 868.68–1801.25 $\times$ 10^3 km^2 $month^{-1}$ on the global scale under the SSP1-2.6-SSP5-8.5 scenario during the mid-term (Table S1). The largest exposure will be in SSP5-8.5, which would be 12.17-fold that of the baseline period, while the lowest would be in SSP1-2.6 (5.87-fold that of the baseline period). The percentage of cropland exposure area to the total cropland area increased from less than 1% in the baseline period to 4.95–8.83% under different scenarios in the middle of the 21st century, and the proportion increased as the emission scenario increased.

For Asia, in the mid-term, the exposure will be 360.92–683.56 $\times$ 10^3 km^2 $month^{-1}$ under the four scenarios (Table S1). The cropland exposure in Africa, North America, Europe, South America, and Oceania will be 249.70–505.60, 69.33–146.91, 79.53–182.67, 93.36–249.20, and 15.83–33.32 $\times$ 10^3 km^2 $month^{-1}$, respectively, under the four scenarios. In all continents, the cropland exposure under SSP1-2.6 will be the lowest, and it will be the largest under the SSP5-8.5 scenario.

From the perspective of spatial distribution, cropland exposure will increase in most regions of the world under SSP scenarios in the middle of the 21st century compared with the baseline period (see Fig. 4). Obvious increases are mainly located in tropical areas such as the South Asian subcontinent, central Africa, most of Europe, and some areas of South America. However, when comparing with the global cultivated land, we find that in the middle of the 21st century, the cultivated land

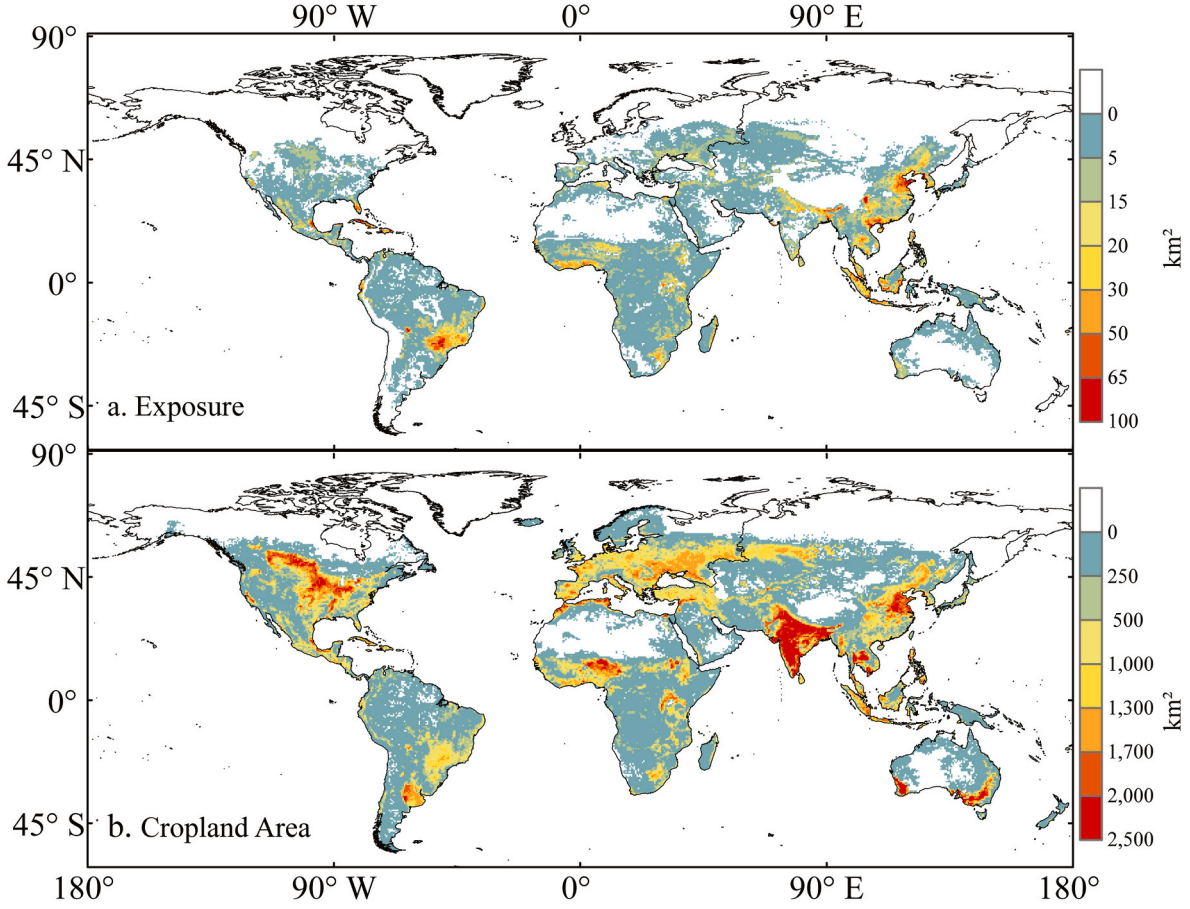

Fig. 3. Global spatial distribution of annual cropland exposure to the extreme CDHEs (a) and the cropland area (b) during the baseline period.

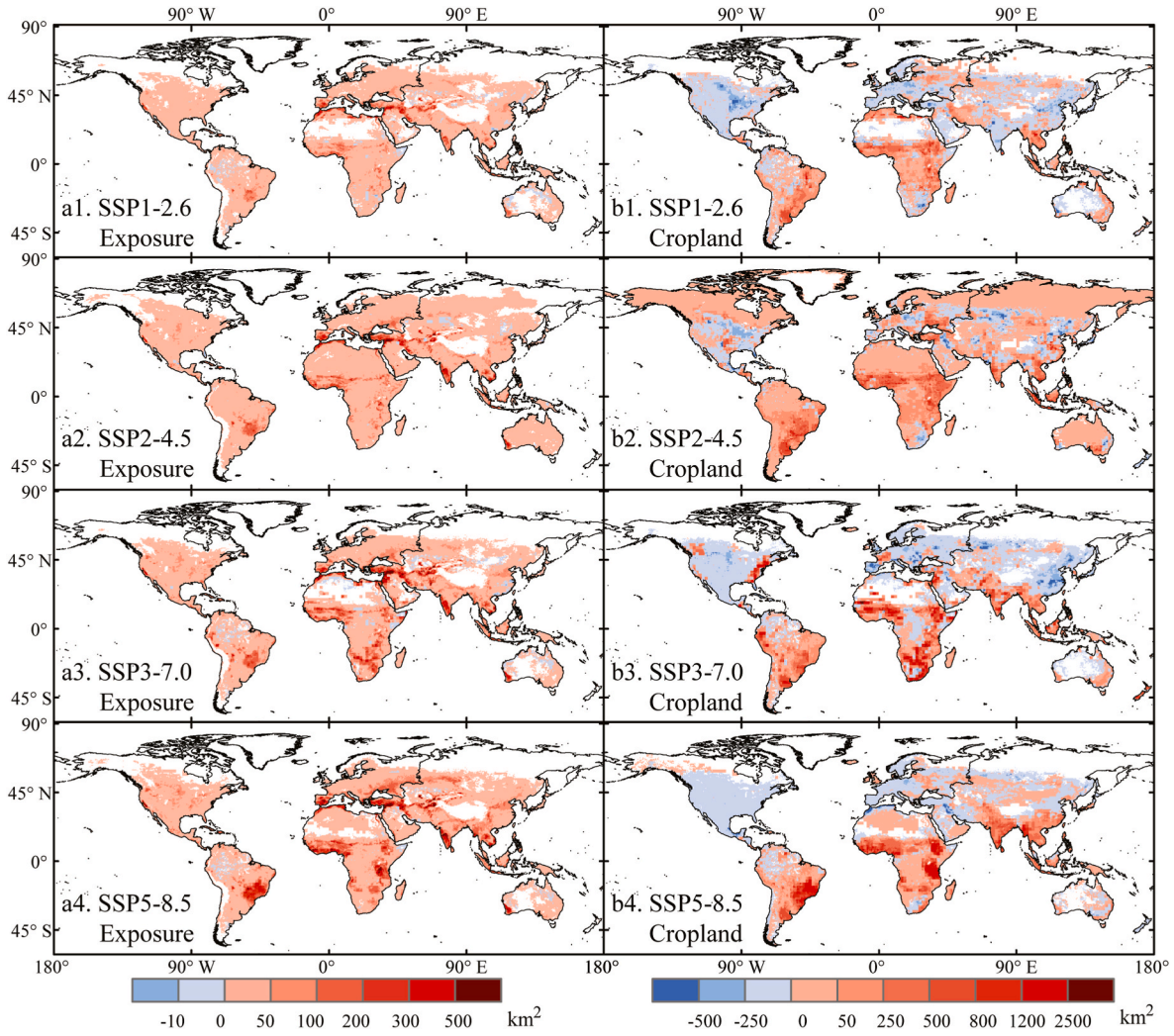

Fig. 4. Changes in cropland exposure to extreme CDHEs (a) and the cropland area (b) in the mid-term under different scenarios compared with the baseline period. The results are based on the 14 CMIP6 multi-model mean.

in North America, eastern China, Europe, and other places will show a decreasing trend compared with the base period, but the exposure degree of cultivated land in this region increased, which is probably caused by the frequent occurrence of extreme CDHEs. However, in South America, Africa, and the South Asian subcontinent, the cultivated land will increase relative to the base period, and the increase in cultivated land exposure in these regions will be mainly caused by the combination of high temperature and drought events and the simultaneous increase in cultivated land.

During the long-term, the global cropland exposure to extreme CDHEs will be 1058.58–3887.54 $\times$ 10^3 km^2 $month^{-1}$ under the SSP scenario (Table S1), an increase of 7.15–26.26-fold compared with the baseline period. The largest proportion of cropland exposure area to the total cropland area will be in SSP5-8.5, accounting for 19.16%, while the lowest will be in SSP1-2.6 (5.28%). All exposure will increase compared with that in the mid-term.

The spatial distribution of cropland exposure is similar to the mid-term; most regions of the world increased compared with the baseline period, especially in the South Asian subcontinent, central Africa, most of Europe, and some areas of South America. The cropland exposure in southern China under the SSP3-7.0 scenario decreased compared with that in the baseline period, and the exposure in other regions increased, especially under the SSP5-8.5 scenario (Fig. 5).

Cropland exposure to extreme CDHEs in the long term of the 21st century in Asia and Africa will be 392.92–1212.96 and 323.06–1429.50 $\times$ 10^3 km^2 $month^{-1}$ under the four scenarios, respectively; the lowest occurred under SSP1-2.6, and the largest will be under SSP3-7.0. The cropland exposure in North America, Europe, South America, and Oceania will be 88.40–450.23, 19.12–105.85, 141.80–459.03, and 93.30–618.46 $\times$ 10^3 km^2 $month^{-1}$ in the four scenarios, respectively. In these four continents, the cropland exposure under SSP1-2.6 will be the lowest, and it will be the largest under the SSP5-8.5 scenario.

Among all continents, exposure of cultivated land in Asia will be the largest, accounting for approximately 40% and 30% of the global total exposure of cultivated land in the middle and end of the 21st century, respectively. The change in cultivated land exposure in Europe will be the most obvious. Under the SSP5-8.5 scenario, the cultivated land exposure in the mid-time and long-term will be 22.84 and 77.33 folds, respectively.

3.4. Relative contribution of climate and cropland changes

To determine the relative importance of various factors to the cropland exposure increase, we categorized the changes in cropland exposure in terms of the effect of climate, cropland, and interactions. Fig. 6 and Fig. 7 show the total changes in cropland exposure and its components over 6 continents and the global scale in the mid-term and long-term under SSP scenarios. Understanding the relative importance of the different drivers of the change in the projected exposure to the extreme CDHEs provides an important means of informing policy

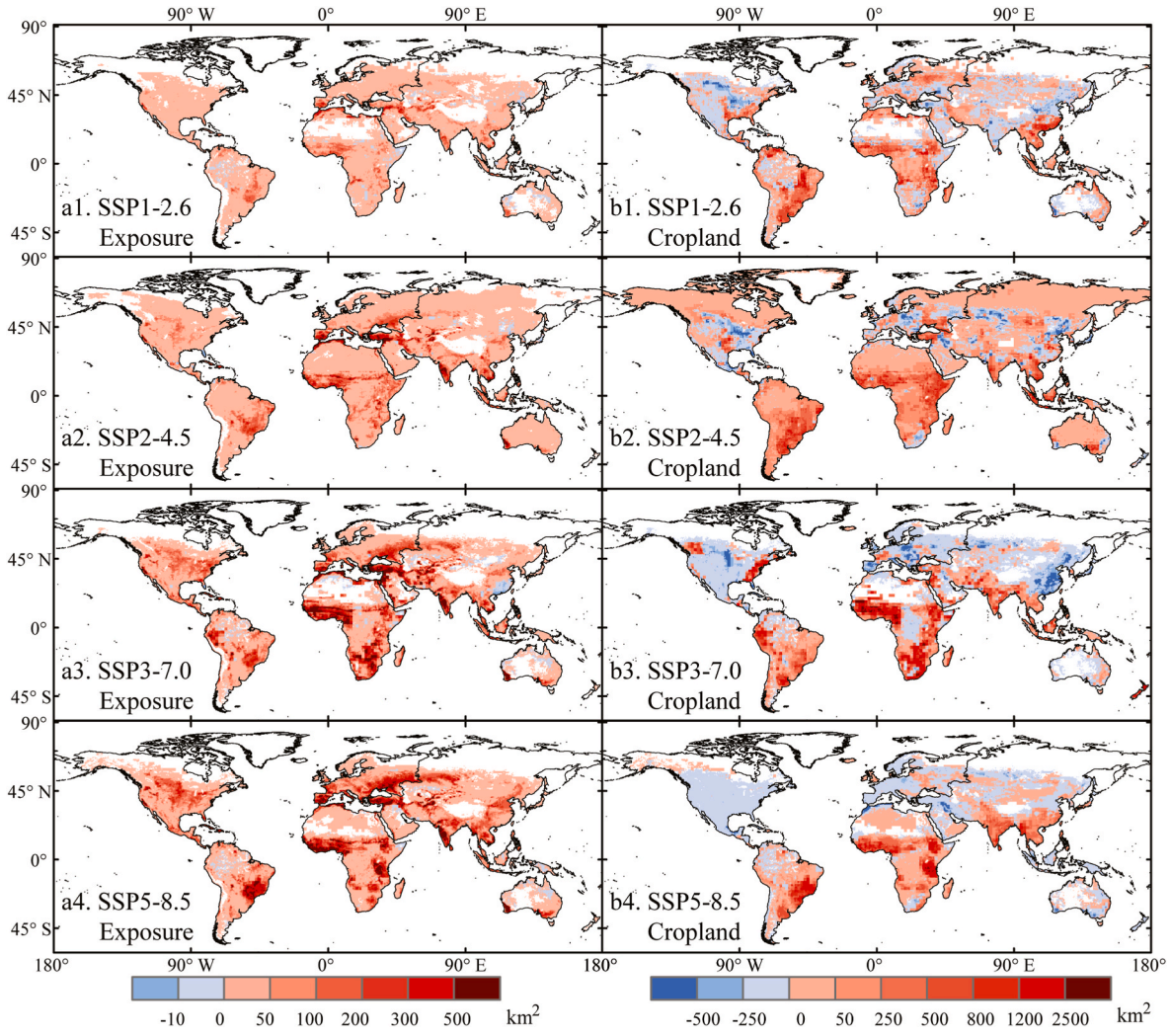

Fig. 5. Changes in cropland exposure to extreme CDHEs (a) and the cropland area (b) in the long-term under different scenarios compared with the baseline period. The results are based on the 14 CMIP6 multi-model ensemble mean.

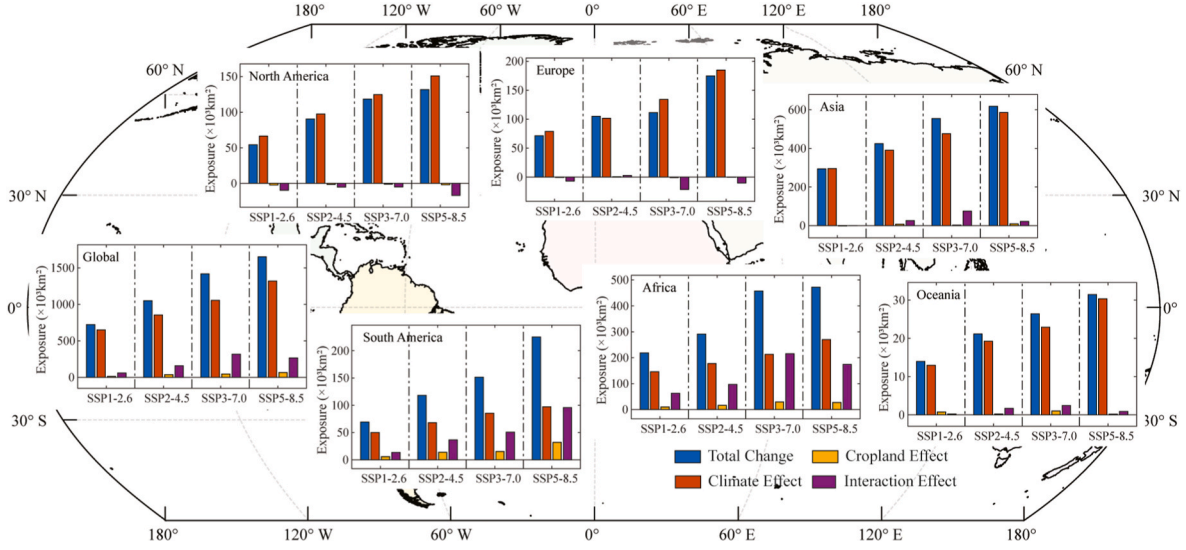

Fig. 6. Decomposition of regional and global projected changes in cropland exposure for the mid-term minus the baseline period. The colored bars are based on the 14 CMIP6 multi-model ensemble mean.

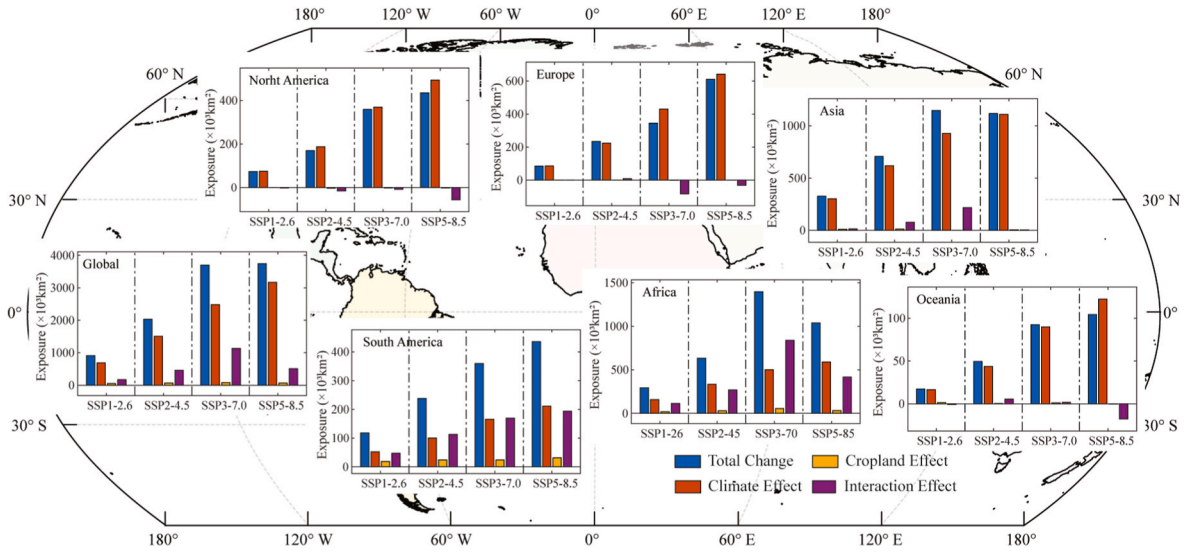

Fig. 7. Decomposition of regional and global projected changes in cropland exposure for the long-term minus the baseline period. The colored bars are based on the 14 CMIP6 multi-model ensemble mean.

responses to dry weather and reducing the exposure of the cropland area.

At the global scale, cropland exposure to extreme CDHEs in the mid-term under the 4 scenarios will be mainly caused by climatic effects (all climatic effects were over 67%). As both the cropland area and the extreme CDHEs frequency increased, the contribution of climatic effect and land-use effect will be positive. For Asia, the contribution of the climate effect in the mid-term under SSP scenarios will be higher than 80%, and under SSP1-2.6, the land-use effect will be negative. The dominant driving factor in the cropland exposure increase will be the climatic effect (see Fig. 6).

As the cropland area in North America will be lower than that of the baseline period under these 4 scenarios, the land-use effects will be negative. As a result, the climatic effect would be more than 100%, which is the dominant effect of the cropland exposure increase. A similar phenomenon also appeared in Europe: land use will be positive (0.45%) in the SSP2-4.5 scenario, and the climatic effect will be more than 100% in the other scenarios.

In South America, climatic effects will be the most important driving factors in increasing exposure to cropland, but the interaction effect increased with the emission scenario, and under SSP5-8.5, the interaction effect will be almost equal to the climatic effect. In Africa, the climatic effect will be over 50% under SSP1-2.6, SSP2-4.5, and SSP5-8.5, while the interaction effect will be slightly higher than the climatic effect. In Oceania, the effect of climate factors will be higher than that of land-use effects.

By the end of the 21st century, due to the increases in the frequency of CDHEs and the area of cropland, the exposure of cropland exposure to extreme CDHEs will be higher than that of the mid-term and baseline period. Climatic effects (75.60%, 74.24%, 67.16%, and 84.65% under SSP126, SSP2-4.5, SSP3-7.0, and SSP5-8.5, respectively) will be the dominant factors causing the cropland exposure increase (see Fig. 7).

The contribution of the climatic effect will be lower than that in the mid-term in Asia, but the land-use effect would be higher. In North America and Europe, the dominant factor (over 70%) will be still the climate effect, while the land-use effects will be negative. For Oceania, the climate effect will be the main driving factor for the cropland exposure increase in the SSP scenarios. For South America, different from the middle term, the interaction effect will be higher than the climate effect in the SSP2-4.5 and SSP3-7.0 scenarios. In Africa, the climatic effect will be over 50% under SSP1-2.6, SSP2-4.5, and SSP5-8.5, while the interaction effect will be slightly higher than the climatic effect.

4. Discussion and conclusion

CDHEs have large impacts on human society, the economy, and natural ecosystems. In this research, we analyze cropland exposure to extreme CDHEs at the global and continental scales under different SSP scenarios from CMIP6 in the mid-term and long-term of the 21st century. This study adopts 14 GCMs, combined with precipitation, potential evapotranspiration, and air temperature, to construct a monthly scale SDHI to evaluate the future temporal and spatial evolution of extreme CDHEs. Combined with LHU2 land-use data, we further analyze the area of cropland exposed to extreme CDHEs under four SSP scenarios.

The high frequency of CDHEs in the historical period is mainly located in Middle and South Asia, the Middle East, North Africa, and northern South America, which are tropical areas. The frequency of extreme CDHEs in the middle and long term of the 21st century will be much higher than that of the baseline period, and the frequency increased along with the increase in emissions. With the continuous rise in global temperature, new risks of extreme CDHEs will emerge in North America, Siberia, and other high-latitude areas in the future. Although the different approaches, datasets, and research periods, the conclusions obtained in our research are basically consistent with the previous research in India (Mishra et al., 2020), China (Yu and Zhai, 2020a, 2020b; Zhang et al., 2021b), and Africa (Weber et al., 2020), and globally (Liu et al., 2021).

According to Liu et al. (2011), relative to 1986–2005, the severity of CDHEs would increase on the global scale and in most regions, such as in Southern Europe, the Mediterranean, North and West of Africa, and the west coast of South America under global warming. However, in their research, only temperature and precipitation are used to determine CDHEs, which ignored the important role of potential evapotranspiration. Meanwhile, their research only chose the SSP5-8.5 scenario, which did not reflect the advantage of multiple scenarios in future projections.

Overall, the global total cropland exposure to extreme CDHEs in warm season during the 1995–2014 period is 148.05 $\times$ 10^3 km^2 $month^{-1}$, accounting for 0.86% of the total cropland. Exposure in the mid-term will be 868.68–1801.25 $\times$ 10^3 km^2 $month^{-1}$ under different SSP scenarios. However, the cropland exposure will be 1058.58–3887.54 $\times$ 10^3 km^2 $month^{-1}$ in the long-term period, and the exposure varied greatly among the different scenarios.

In the baseline period, cropland exposure to extreme CDHEs in Asia

is the largest, followed by that in Africa, South America, and Europe. In the middle and long term of the 21st century, cropland exposure will be much higher than that in the baseline period. Exposure in Asia will be still the largest, except in the SSP3-7.0 scenario in the long term. In addition, cropland exposure to extreme CDHEs in Africa increased obviously. In the mid-term, cropland exposure in Africa increased from 31.17×10^3 km^2 month^{-1} to 249.70–505.60 $\times 10^3$ km^2 month^{-1}. At the global and continental scales, it will be clear that the frequencies of CDHEs and cropland exposure will be the lowest under the low-emission scenario compared with the high-emission scenarios. Maintaining the low-emission scenario can effectively reduce the impact of CDHEs in cropland.

Africa is particularly exposed and vulnerable to a wide range of different climate risks. Policymakers seeking to understand the climate risks faced by Africa in a changing climate, therefore, need information on the climate hazards, exposure of assets, and vulnerability if they are to plan and adapt effectively. The CDHEs population exposure in Africa projected a strong increase in exposure (Weber et al., 2020; Liu et al., 2021). The strongest growth of population exposure is simulated for West Africa (2.2 billion person-events), Central-East Africa (1.7 billion person-events), and Northeast Africa (1.0 billion person-events) under the RCP8.5/SSP3 scenario (Weber et al., 2020). Combined with our research, the population and cropland exposed to CDHEs would increase obviously, which will greatly increase the risk of food shortages in the region and add a heavier burden to this already fragile region. As such, the policymakers responsible for adaptation planning will be facing increasing risks over the course of this century (Weber et al., 2020).

South Asia has a high density of cropland in the world, contains one of the largest irrigation systems (Immerzeel et al., 2010; Su et al., 2016), and is vulnerable to drought and heatwave events, which is sensitive to the reduction in water supply and threaten food security. In contrast to Africa, irrigated agriculture in South Asia depends on meltwater, monsoon rains, and groundwater (Lutz et al., 2022). Research has shown that the drought (Wen et al., 2019; Wang et al., 2020; Zhai et al., 2020; Mondal et al., 2021), heatwaves (Luo and Lau, 2018; Ullah et al., 2022) and CDHEs (Mishra et al., 2020; Das et al., 2022) in South Asia would increase. In terms of population exposure to CDHEs, the multi-model mean projects 2.25- to 3.11-fold, 2.51- to 4.96-fold, and 2.14- to 2.70-fold increase in the number of person-events with respect to the historical period (65.20 billion person-events) under SSP2-4.5, SSP3-7.0, and SSP5-8.5, respectively (Das et al., 2022). The increase in extreme CDHEs and cropland areas lead to a continuous increase in cropland exposure to extreme CDHEs, which seriously threatened the local water supply and food security, increasing the importance of meltwater and groundwater to irrigated agriculture.

Although our research provides valuable information for future changes in extreme CDHEs at the global and continental scales, it should be acknowledged that the conclusions are limited in some places. In this study, a monthly SDHI that used precipitation, potential evapotranspiration, and temperature to reflect extreme CDHEs is defined for the warm season to reflect dry-hot conditions in the world. This is different from previous studies, which were based on precipitation and temperature and ignored the effect of potential evapotranspiration on drought (Hao et al., 2018; Wu et al., 2020; Liu et al., 2021; Tang et al., 2022). Potential evapotranspiration represents the regional evaporative capacity and plays a pivotal role in the drying process (Wen et al., 2019; Wang et al., 2020). It is important to choose a suitable method to calculate potential evapotranspiration for drought assessment (Zhou et al., 2020). The potential evapotranspiration method used in our research was the Thornthwaite evapotranspiration formula, which was the simplest method and considered only the temperature (Vicente-Serrano et al., 2010) and will provide underestimates in arid and semiarid regions and overestimates in humid regions (Wen et al., 2019; Wang et al., 2020; Zhou et al., 2020). Many studies have shown that the Penman-Monteith equation, which incorporates the multiple effects of thermal and dynamic factors, could be considered the best method of drought assessment (Su et al., 2018; Wen et al., 2019; Wang et al., 2020; Zhou et al., 2020).

Another area that needs to be improved in future research is the refinement of the time scale. In traditional studies, drought is generally defined on a monthly scale, but at present, research on drought has begun to focus on the study of flash droughts on a daily scale (Yuan et al., 2019). Flash drought is a new type of drought. Compared with traditional droughts, flash droughts develop more rapidly and have a shorter forecast period. In the future, we would focus on the research of the CDHEs on a daily scale.

Declaration of competing interest

The authors declare that they have no known competing financial interests or personal relationships that could have appeared to influence the work reported in this paper.

Data availability

Data will be made available on request.

Acknowledgments

This work was supported by the Natural Science Foundation of Shandong Province, China (ZR2021QD139), the Postdoctoral Innovation Project of Shandong Province (2021BHCX54), and the National Science Foundation of China (41971023).

Appendix A. Supplementary data

Supplementary data to this article can be found online at https://doi.org/10.1016/j.wace.2023.100559.

References

AghaKouchak, A., Cheng, L., Mazdiyasni, O., Farahmand, A., 2014. Global warming and changes in risk of concurrent climate extremes: insights from the 2014 California drought. Geophys. Res. Lett. 41 (24), 8847–8852. https://doi.org/10.1002/2014GL062308.

Alizadeh, M.R., Adamowski, J., Nikoo, M.R., AghaKouchak, A., Dennison, P., Sadegh, M., 2020. A century of observations reveals increasing likelihood of continental-scale compound dry-hot extremes. Sci. Adv. 6 (39), eaaz4571. https://doi.org/10.1126/sciadv.aaz4571.

Chen, J., Liu, Y., Pan, T., Liu, Y., Sun, F., Ge, Q., 2018. Population exposure to droughts in China under the 1.5°C global warming target. Copernicus Publications Earth System Dynamics 9 (3), 1097–1106. https://doi.org/10.5194/esd-9-1097-2018.

Chen, J., Liu, Y., Pan, T., Ciais, P., Ma, T., Liu, Y., Yamazaki, D., Ge, Q., Peñuelas, J., 2020a. Global socioeconomic exposure of heat extremes under climate change. J. Clean. Prod. 277, 123275 https://doi.org/10.1016/j.jclepro.2020.123275.

Chen, M., Vernon, C.R., Graham, N.T., Hejazi, M., Huang, M., Cheng, Y., Calvin, K., 2020b. Global land use for 2015–2100 at 0.05° resolution under diverse socioeconomic and climate scenarios. Nature Research Scientific Data 7 (1). https://doi.org/10.1038/s41597-020-00669-x.

Das, J., Manikanta, V., Umamahesh, N.V., 2022. Population exposure to compound extreme events in India under different emission and population scenarios. Sci. Total Environ. 806, 150424 https://doi.org/10.1016/j.scitotenv.2021.150424.

Eyring, V., Bony, S., Meehl, G.A., Senior, C.A., Stevens, B., Stouffer, R.J., Taylor, K.E., 2016. Overview of the coupled model Intercomparison project Phase 6 (CMIP6) experimental design and organization. Geosci. Model Dev. (GMD) 9 (5), 1937–1958. https://doi.org/10.5194/gmd-9-1937-2016.

Feng, S., Hao, Z., Zhang, X., Hao, F., 2019. Probabilistic evaluation of the impact of compound dry-hot events on global maize yields. Sci. Total Environ. 689, 1228–1234. https://doi.org/10.1016/j.scitotenv.2019.06.373.

Feng, Y., Liu, W., Sun, F., Wang, H., 2021. Changes of compound hot and dry extremes on different land surface conditions in China during 1957–2018. Int. J. Climatol. 41 (S1), E1085–E1099. https://doi.org/10.1002/joc.6755.

García-Peña, G.E., Rubio, A.V., Mendoza, H., Fernández, M., Milholland, M.T., Aguirre, A.A., Suzán, G., Zambrana-Torrelio, C., 2021. Land-use change and rodent-borne diseases: hazards on the shared socioeconomic pathways. Phil. Trans. Biol. Sci. 376 (1837), 20200362 https://doi.org/10.1098/rstb.2020.0362. The Royal Society.

Gidden, M.J., Riahi, K., Smith, S.J., Fujimori, S., Luderer, G., Kriegler, E., van Vuuren, D. P., van den Berg, M., Feng, L., Klein, D., Calvin, K., Doelman, J.C., Frank, S., Fricko, O., Harmsen, M., Hasegawa, T., Havlik, P., Hilaire, J., Hoesly, R., Horing, J., Popp, A., Stehfest, E., Takahashi, K., 2019. Global emissions pathways under different socioeconomic scenarios for use in CMIP6: a dataset of harmonized

emissions trajectories through the end of the century. Geosci. Model Dev. (GMD) 12 (4), 1443–1475. https://doi.org/10.5194/gmd-12-1443-2019.
Gringorten II., 1963. A plotting rule for extreme probability paper. J. Geophys. Res. 68 (3), 813–814. https://doi.org/10.1029/JZ068i003p00813.
Hao, Z., Hao, F., Singh, V.P., Zhang, X., 2018. Changes in the severity of compound drought and hot extremes over global land areas. Environ. Res. Lett. 13 (12), 124022 https://doi.org/10.1088/1748-9326/aaee96.
Hao, Z., Hao, F., Singh, V.P., Zhang, X., 2019. Statistical prediction of the severity of compound dry-hot events based on El Niño-Southern Oscillation. J. Hydrol. 572, 243–250. https://doi.org/10.1016/j.jhydrol.2019.03.001.
Hao, Z., Hao, F., Singh, V.P., Ouyang, W., Zhang, X., Zhang, S., 2020. A joint extreme index for compound droughts and hot extremes. Theor. Appl. Climatol. 142 (1), 321–328. https://doi.org/10.1007/s00704-020-03317-x.
Harris, I., Osborn, T.J., Jones, P., Lister, D., 2020. Version 4 of the CRU TS monthly high-resolution gridded multivariate climate dataset. Sci. Data 7 (1), 109. https://doi.org/10.1038/s41597-020-0453-3.
He, Y., Fang, J., Xu, W., Shi, P., 2022a. Substantial increase of compound droughts and heatwaves in wheat growing seasons worldwide. Int. J. Climatol. https://doi.org/10.1002/joc.7518 n/a(n/a): 1–17.
He, Y., Hu, X., Xu, W., Fang, J., Shi, P., 2022b. Increased probability and severity of compound dry and hot growing seasons over world's major croplands. Sci. Total Environ. 824, 153885 https://doi.org/10.1016/J.SCITOTENV.2022.153885. Elsevier.
Hofer, S., Lang, C., Amory, C., Kittel, C., Delhasse, A., Tedstone, A., Fettweis, X., 2020. Greater Greenland Ice Sheet contribution to global sea level rise in CMIP6. Nat. Commun. 11 (1), 6289. https://doi.org/10.1038/s41467-020-20011-8.
Hu, Q., Xiang, M., Chen, D., Zhou, J., Wu, W., Song, Q., 2020. Global cropland intensification surpassed expansion between 2000 and 2010: a spatio-temporal analysis based on GlobeLand30. Sci. Total Environ. 746, 141035 https://doi.org/10.1016/j.scitotenv.2020.141035.
Hurtt, G.C., Chini, L., Sahajpal, R., Frolking, S., Bodirsky, B.L., Calvin, K., Doelman, J.C., Fisk, J., Fujimori, S., Goldewijk, K.K., Hasegawa, T., Havlik, P., Heinimann, A., Humpenöder, F., Jungclaus, J., Kaplan, J.O., Kennedy, J., Krisztin, T., Lawrence, D., Lawrence, P., Ma, L., Mertz, O., Pongratz, J., Popp, A., Poulter, B., Riahi, K., Shevliakova, E., Stehfest, E., Thornton, P., Tubiello, F.N., van Vuuren, D.P., Zhang, X., 2020. Harmonization of global land use change and management for the period 850-2100 (LUH2) for CMIP6. Copernicus GmbH Geoscientific Model Development 13 (11), 5425–5464. https://doi.org/10.5194/gmd-13-5425-2020.
Immerzeel, W.W., van Beek, L.P.H., Bierkens, M.F.P., 2010. Climate change will affect the Asian water towers. Science 328 (5984), 1382–1385. https://doi.org/10.1126/science.1183188.
IPCC, 2021. Summary for policymakers. In: Masson-Delmotte, V., Zhai, P., Pirani, A., Connors, S.L., Péan, C., Berger, S., Caud, N., Chen, Y., Goldfarb, L., Gomis, M.I., Huang, M., Leitzell, K., Lonnoy, E., Matthews, J.B.R., Maycock, T.K., Waterfield, T., Yelekçi, O., Yu, R., Zhou, B. (Eds.), Climate Change 2021: the Physical Science Basis. Contribution of Working Group I to the Sixth Assessment Report of the Intergovernmental Panel on Climate Change. Cambridge University Press, Cambridge, United Kingdom and New York, NY, USA, pp. 3–32. https://doi.org/10.1017/9781009157896.001.
Jones, B., O'Neill, B.C., Mcdaniel, L., Mcginnis, S., Mearns, L.O., Tebaldi, C., 2015. Future population exposure to US heat extremes. Nat. Clim. Change 5 (7), 652–655. https://doi.org/10.1038/nclimate2631.
Jones, B., Tebaldi, C., O'Neill, B.C., Oleson, K., Gao, J., 2018. Avoiding population exposure to heat-related extremes: demographic change vs climate change. Climatic Change 146 (3–4), 423–437. https://doi.org/10.1007/s10584-017-2133-7.
Leonard, M., Westra, S., Phatak, A., Lambert, M., van den Hurk, B., McInnes, K., Risbey, J., Schuster, S., Jakob, D., Stafford-Smith, M., 2014. A compound event framework for understanding extreme impacts. WIREs Climate Change 5 (1), 113–128. https://doi.org/10.1002/wcc.252.
Lesk, C., Anderson, W., 2021. Decadal variability modulates trends in concurrent heat and drought over global croplands. Environ. Res. Lett. 16 (5), 55024 https://doi.org/10.1088/1748-9326/abeb35.
Lesk, C., Rowhani, P., Ramankutty, N., 2016. Influence of extreme weather disasters on global crop production. Nature 529 (7584), 84–87. https://doi.org/10.1038/nature16467.
Li, H., Sheffield, J., Wood, E.F., 2010. Bias correction of monthly precipitation and temperature fields from Intergovernmental Panel on Climate Change AR4 models using equidistant quantile matching. J. Geophys. Res. Atmos. 115 (D10) https://doi.org/10.1029/2009JD012882.
Li, W., Jiang, Z., Li, L.Z.X., Luo, J.-J., Zhai, P., 2022. Detection and attribution of changes in summer compound hot and dry events over Northeastern China with CMIP6 models. J. Meteorol. Res. 36 (1), 37–48. https://doi.org/10.1007/s13351-022-1112-8.
Libonati, R., Geirinhas, J.L., Silva, P.S., Russo, A., Rodrigues, J.A., Belém, L.B.C., Nogueira, J., Roque, F.O., DaCamara, C.C., Nunes, A.M.B., Marengo, J.A., Trigo, R. M., 2022. Assessing the role of compound drought and heatwave events on unprecedented 2020 wildfires in the Pantanal. Environ. Res. Lett. 17 (1), 15005 https://doi.org/10.1088/1748-9326/ac462e.
Liu, Z., Anderson, B., Yan, K., Dong, W., Liao, H., Shi, P., 2017. Global and regional changes in exposure to extreme heat and the relative contributions of climate and population change. Sci. Rep. 7 (1), 43909 https://doi.org/10.1038/srep43909.
Liu, W., Sun, F., Feng, Y., Li, C., Chen, J., Sang, Y.F., Zhang, Q., 2021. Increasing population exposure to global warm-season concurrent dry and hot extremes under different warming levels. Environ. Res. Lett. 16 (9), 94002 https://doi.org/10.1088/1748-9326/ac188f.
Luo, M., Lau, N.-C., 2018. Synoptic characteristics, atmospheric controls, and long-term changes of heat waves over the Indochina Peninsula. Clim. Dynam. 51 (7), 2707–2723. https://doi.org/10.1007/s00382-017-4038-6.
Luo, M., Lau, N.-C., Liu, Z., Wu, S., Wang, X., 2022. An observational investigation of spatiotemporally contiguous heatwaves in China from a 3D perspective. Geophys. Res. Lett. 49 (6), e2022GL097714 https://doi.org/10.1029/2022GL097714.
Lutz, A.F., Immerzeel, W.W., Siderius, C., Wijngaard, R.R., Nepal, S., Shrestha, A.B., Wester, P., Biemans, H., 2022. South Asian agriculture increasingly dependent on meltwater and groundwater. Nat. Clim. Change. https://doi.org/10.1038/s41558-022-01355-z.
Ma, F., Yuan, X., 2021. Impact of climate and population changes on the increasing exposure to summertime compound hot extremes. Sci. Total Environ. 772, 145004 https://doi.org/10.1016/j.scitotenv.2021.145004.
Ma, L., Hurtt, G.C., Chini, L.P., Sahajpal, R., Pongratz, J., Frolking, S., Stehfest, E., Klein Goldewijk, K., O'Leary, D., Doelman, J.C., 2020. Global rules for translating land-use change (LUH2) to land-cover change for CMIP6 using GLM2. Geosci. Model Dev. (GMD) 13 (7), 3203–3220. https://doi.org/10.5194/gmd-13-3203-2020.
Mazdiyasni, O., AghaKouchak, A., 2015. Substantial increase in concurrent droughts and heatwaves in the United States. Proc. Natl. Acad. Sci. U. S. A 112 (37), 11484–11489. https://doi.org/10.1073/pnas.1422945112.
McKee, T.B., Doesken, N.J., Kleist, J.R., 1993. The Relationship of Drought Frequency and Duration to Time Scales.
Miralles, D.G., Gentine, P., Seneviratne, S.I., Teuling, A.J., 2019. Land-atmospheric feedbacks during droughts and heatwaves: state of the science and current challenges. John Wiley and Sons Inc. Ann. N. Y. Acad. Sci. 1436 (1), 19–35. https://doi.org/10.1111/nyas.13912.
Mishra, V., Thirumalai, K., Singh, D., Aadhar, S., 2020. Future exacerbation of hot and dry summer monsoon extremes in India. npj Climate and Atmospheric Science 3 (1), 10. https://doi.org/10.1038/s41612-020-0113-5.
Mondal, S.K., Huang, J., Wang, Y., Su, B., Zhai, J., Tao, H., Wang, G., Fischer, T., Wen, S., Jiang, T., 2021. Doubling of the population exposed to drought over South Asia: CMIP6 multi-model-based analysis. Sci. Total Environ. 771, 145186 https://doi.org/10.1016/j.scitotenv.2021.145186.
Mukherjee, S., Ashfaq, M., Mishra, A.K., 2020. Compound drought and heatwaves at a global scale: the role of natural climate variability-associated synoptic patterns and land-surface energy budget anomalies. J. Geophys. Res. Atmos. 125 (11), e2019JD031943 https://doi.org/10.1029/2019JD031943.
Potapov, P., Turubanova, S., Hansen, M.C., Tyukavina, A., Zalles, V., Khan, A., Song, X.-P., Pickens, A., Shen, Q., Cortez, J., 2022. Global maps of cropland extent and change show accelerated cropland expansion in the twenty-first century. Nature Food 3 (1), 19–28. https://doi.org/10.1038/s43016-021-00429-z.
Ray, D.K., Gerber, J.S., MacDonald, G.K., West, P.C., 2015. Climate variation explains a third of global crop yield variability. Nat. Commun. 6 (1), 5989. https://doi.org/10.1038/ncomms6989.
Seneviratne, S.I., Corti, T., Davin, E.L., Hirschi, M., Jaeger, E.B., Lehner, I., Orlowsky, B., Teuling, A.J., 2010. Investigating soil moisture–climate interactions in a changing climate: a review. Earth Sci. Rev. 99 (3), 125–161. https://doi.org/10.1016/j.earscirev.2010.02.004.
Siebert, S., Webber, H., Zhao, G., Ewert, F., 2017. Heat stress is overestimated in climate impact studies for irrigated agriculture. Environ. Res. Lett. 12 (5), 54023 https://doi.org/10.1088/1748-9326/aa702f.
Smirnov, O., Zhang, M., Xiao, T., Orbell, J., Lobben, A., Gordon, J., 2016. The relative importance of climate change and population growth for exposure to future extreme droughts. Climatic Change 138 (1–2), 41–53. https://doi.org/10.1007/s10584-016-1716-z.
Song, Y., Lv, M., Wang, M., Li, X., Qu, Y., 2021. Reconstruction of historical land surface albedo changes in China from 850 to 2015 using land use harmonization data and albedo look-up maps. Earth Space Sci. 8 (9), e2021EA001799 https://doi.org/10.1029/2021EA001799.
Su, B., Huang, J., Gemmer, M., Jian, D., Tao, H., Jiang, T., Zhao, C., 2016. Statistical downscaling of CMIP5 multi-model ensemble for projected changes of climate in the Indus River Basin. Atmos. Res. 178–179, 138–149. https://doi.org/10.1016/j.atmosres.2016.03.023.
Su, B., H, J., F, T., W, Y., W K, Z., Z, J., S, H., Wang, A., Zeng, X., W, G., T, H., G, M., Li, X., J, T., 2018. Drought losses in China might double between the 1.5 degrees C and 2.0 degrees C warming. Proc. Natl. Acad. Sci. U. S. A. 115 (42), 10600–10605. https://doi.org/10.1073/pnas.1802129115.
Tang, Z.I., Yang, T.I., Lin, X., Li, X., Cao, R., Li, W., 2022. Future changes in the risk of compound hot and dry events over China estimated with two large ensembles. PLoS One 17 (3), e0264980. https://doi.org/10.1371/journal.pone.0264980.
Thornthwaite, C.W., 1948. An approach toward a rational classification of climate. Soil Sci. 66, 55–94.
Ullah, I., Saleem, F., Iyakaremye, V., Yin, J., Ma, X., Syed, S., Hina, S., Asfaw, T.G., Omer, A., 2022. Projected changes in socioeconomic exposure to heatwaves in South Asia under changing climate. Earth's Future 10 (2), e2021EF002240. https://doi.org/10.1029/2021ef002240.
Vicente-Serrano, S.M., Beguería, S., López-Moreno, J.I., 2010. A multiscalar drought index sensitive to global warming: the standardized precipitation evapotranspiration index. J. Clim. 23 (7), 1696–1718. https://doi.org/10.1175/2009JCLI2909.1. American Meteorological Society: Boston MA, USA.
Wang, A., Wang, Y., Su, B., Kundzewicz, Z.W., Tao, H., Wen, S., Qin, J., Gong, Y., Jiang, T., 2020. Comparison of changing population exposure to droughts in river basins of the Tarim and the Indus. Earth's Future 8 (5), e2019EF001448. https://doi.org/10.1029/2019EF001448.
Wang, A., Tao, H., Wu, Q., Huang, J., Zhang, B., Wang, Y., 2022. Increasing urban and rural population exposures to warm-season concurrent hot days and nights on the

North China Plain. Int. J. Climatol. 42 (15), 7938–7950. https://doi.org/10.1002/joc.7685.
Weber, T., Bowyer, P., Rechid, D., Pfeifer, S., Raffaele, F., Remedio, A.R., Teichmann, C., Jacob, D., 2020. Analysis of compound climate extremes and exposed population in Africa under two different emission scenarios. Earth's Future 8 (9), e2019EF001473. https://doi.org/10.1029/2019EF001473.
Wen, S., Wang, A., Tao, H., Malik, K., Huang, J., Zhai, J., Jing, C., Rasul, G., Su, B., 2019. Population exposed to drought under the 1.5 °C and 2.0 °C warming in the Indus river basin. Atmos. Res. 218, 296–305. https://doi.org/10.1016/j.atmosres.2018.12.003.
Willmott, C.J., Rowe, C.M., Mintz, Y., 1985. Climatology of the terrestrial seasonal water cycle. J. Climatol. 5 (6), 589–606. https://doi.org/10.1002/joc.3370050602.
Wu, X., Jiang, D., 2022. Probabilistic impacts of compound dry and hot events on global gross primary production. Environ. Res. Lett. 17 (3), 34049 https://doi.org/10.1088/1748-9326/ac4c5b.
Wu, X., Hao, Z., Zhang, X., Li, C., Hao, F., 2020. Evaluation of severity changes of compound dry and hot events in China based on a multivariate multi-index approach. J. Hydrol. 583, 124580 https://doi.org/10.1016/j.jhydrol.2020.124580. Elsevier.
Yu, R., Zhai, P., 2020a. More frequent and widespread persistent compound drought and heat event observed in China. Sci. Rep. 10 (1), 14576 https://doi.org/10.1038/s41598-020-71312-3.
Yu, R., Zhai, P., 2020b. Changes in compound drought and hot extreme events in summer over populated eastern China. Weather Clim. Extrem. 30, 100295 https://doi.org/10.1016/j.wace.2020.100295.
Yuan, X., Wang, L., Wu, P., Ji, P., Sheffield, J., Zhang, M., 2019. Anthropogenic shift towards higher risk of flash drought over China. Nat. Commun. 10 (1), 4661. https://doi.org/10.1038/s41467-019-12692-7.
Zhai, J., Mondal, S.K., Fischer, T., Wang, Y., Su, B., Huang, J., Tao, H., Wang, G., Ullah, W., Uddin, M.J., 2020. Future drought characteristics through a multi-model ensemble from CMIP6 over South Asia. Atmos. Res. 246, 105111 https://doi.org/10.1016/j.atmosres.2020.105111.
Zhang, W., Luo, M., Gao, S., Chen, W., Hari, V., Khouakhi, A., 2021a. Compound hydrometeorological extremes: drivers, mechanisms and methods. Front. Earth Sci. 9 https://doi.org/10.3389/feart.2021.673495.
Zhang, Y., Mao, G., Chen, C., Shen, L., Xiao, B., 2021b. Population exposure to compound droughts and heatwaves in the observations and era 5 reanalysis data in the gan river basin, China. Land 10 (10), 1021. https://doi.org/10.3390/land10101021.
Zhang, Q., She, D., Zhang, L., Wang, G., Chen, J., Hao, Z., 2022a. High sensitivity of compound drought and heatwave events to global warming in the future. Earth's Future 10 (11). https://doi.org/10.1029/2022ef002833.
Zhang, Y., Hao, Z., Zhang, X., Hao, F., 2022b. Anthropogenically forced increases in compound dry and hot events at the global and continental scales. Environ. Res. Lett. 17 (2), 24018 https://doi.org/10.1088/1748-9326/ac43e0.
Zhou, J., Wang, Y., Su, B., Wang, A., Tao, H., Zhai, J., Kundzewicz, Z.W., Jiang, T., 2020. Choice of potential evapotranspiration formulas influences drought assessment: a case study in China. Atmos. Res. 242, 104979 https://doi.org/10.1016/j.atmosres.2020.104979.
Zscheischler, J., Seneviratne, S.I., 2017. Dependence of drivers affects risks associated with compound events. Sci. Adv. 3 (6), e1700263 https://doi.org/10.1126/sciadv.1700263.
Zscheischler, J., Westra, S., van den Hurk, B.J.J.M., Seneviratne, S.I., Ward, P.J., Pitman, A., AghaKouchak, A., Bresch, D.N., Leonard, M., Wahl, T., Zhang, X., 2018. Future climate risk from compound events. Nat. Clim. Change 8 (6), 469–477. https://doi.org/10.1038/s41558-018-0156-3.
Zscheischler, J., Martius, O., Westra, S., Bevacqua, E., Raymond, C., Horton, R.M., van den Hurk, B., AghaKouchak, A., Jézéquel, A., Mahecha, M.D., Maraun, D., Ramos, A. M., Ridder, N.N., Thiery, W., Vignotto, E., 2020. A typology of compound weather and climate events. Nat. Rev. Earth Environ. 1 (7), 333–347. https://doi.org/10.1038/s43017-020-0060-z.